applied sciences

MDPI

Article

Combustion and Performance Study of Low-Displacement Compression Ignition Engines Operating with Diesel–Biodiesel Blends

Guillermo Valencia Ochoa [1], Carlos Acevedo Peñaloza [2] and Jorge Duarte Forero [1,*]

[1] Programa de Ingeniería Mecánica, Universidad del Atlántico, Carrera 30 Número 8-49, Puerto Colombia, Barranquilla 080007, Colombia; guillermoevalencia@mail.uniatlantico.edu.co

[2] Facultad de Ingeniería, Universidad Francisco de Paula Santander, Avenida Gran Colombia No. 12E-96 Barrio Colsag, Cúcuta 540003, Colombia; carloshumbertoap@ufps.edu.co

* Correspondence: jorgeduarte@mail.uniatlantico.edu.co; Tel.: +575-3853002

Received: 9 November 2019; Accepted: 21 January 2020; Published: 30 January 2020

Abstract: This study investigated the influence of different biodiesel blends produced from residual sunflower oil and palm oil from agroindustry liquid waste on the characteristics of the combustion process, performance, and emissions in a single-cylinder diesel engine. For the analysis of the combustion process, a diagnostic model was developed based on the cylinder pressure signal, which allows the calculation of the heat release rate, the accumulated heat rate, and the temperature in the combustion chamber. This is to assess the influence of these parameters on engine emissions. The experiments on the diesel engine were carried out using five types of fuel: conventional diesel, two biodiesel blends of residual palm oil (PB5 and PB10), and two biodiesel blends formed with palm oil and sunflower oil residues (PB5SB5 and PB10SB5). The engine was running in four different modes, which covered its entire operating area. Experimental results show that the in-cylinder pressure curves decrease as the percentage of biodiesel in the fuel increases. Similarly, the results showed a decrease in the heat release rate for biodiesel blends. The diagrams of the accumulated heat release curves were larger for fuels with higher biodiesel content. This effect is reflected in the thermal efficiency of biodiesel blends since the maximum thermal efficiencies were 29.4%, 30%, 30.6%, 31.2%, and 31.8% for PB10SB5, PB5SB5, PB10, PB5, and diesel, respectively. The emission analysis showed that the blends of biodiesel PB5SB5 and PB10SB allowed a greater reduction in the emissions of CO, CO_2, HC, and opacity of smoke in all the modes of operation tested, in comparison with the blends of biodiesel PB5 and PB10. However, NOx emissions increased. In general, biodiesel with the percentage of residual sunflower oil does not cause a significant change in the combustion process and engine performance, when compared to biodiesel that includes only residual palm oil.

Keywords: biodiesel; combustion process; emissions; diesel engine; thermodynamic model

1. Introduction

The industrial growth and modernization of the world have progressively caused the depletion of fossil resources and serious environmental problems, which has led to a global interest in the search for alternative fuels that can be used in diesel engines. These new fuels must be characterized by coming from renewable resources, minimizing environmental impact, and being economically viable [1,2]. Biodiesel appears to be a promising solution, as it allows the continued use of existing technology of internal combustion engines, either purely or combined with diesel [3]. Other advantages of using biodiesel are its lower sulfur and aromatic content, and higher flash point compared to diesel. These characteristics make biodiesel safer to handle, and biodegradable [4]. In addition, its chemical

composition contributes to a reduction in carbon monoxide, carbon dioxide, hydrocarbons, and soot emissions [5].

Among the different products for the production of biodiesel, palm oil stands out due to its properties similar to diesel from regular petroleum [6,7]. These characteristics have caused the biodiesel derived from palm oil to be been widely investigated. However, the use of edible vegetable oils is related to environmental problems, such as deforestation, soil destruction, and consumption of much of the arable land [8]. In addition, biofuels are criticized for the use of feedstocks that could also be used as food resources. Therefore, not all of them are economically profitable, as they can be considered to be food crops [9]. Because of this, the selection of edible vegetable oils as a potential biodiesel feedstock cannot be considered a long-term option.

A researched alternative is the production of biodiesel through the use of residual palm oil, which can eliminate the problems associated with the use of edible oils and reduce pollution from this type of waste [10]. In particular, the palm oil industry produces a large amount of waste in the liquid or solid form [11]. It is reported that only 10% of the biomass produced in palm oil farms is converted for edible use; the remaining 90% is polluting waste material [12,13]. Among the by-products of palm, oil residues are residual palm oil, fatty acid residues, residual oil from the empty futon cluster, residual oil from the palm decanter cake, and industrial liquid waste [14]. The use of palm oil residues, in addition to positively impacting the environment, have certain economic advantages. Studies show that the cost of production of palm oil residues is 20% to 30% lower when compared to refined vegetable oil [15], the raw material is abundant and at a reduced price [16].

Additionally, a large amount of waste from used cooking oil (UCO) is progressively generated by homes, restaurants, and food processing industries. This type of waste has been investigated for the production of biodiesel [17–19]. However, the higher content of fatty acids, the percentage of water, and the lower calorific value compared to standard diesel have caused a reduction in the viability of using UCO as a raw material for the production of biodiesel [14]. Due to the above, alternative forms are required for the use of UCO as a raw material in the generation of biodiesel, which would contribute to the reduction of pollution problems associated with the UCO.

Among the different types of residual cooking oils, sunflower oil has a relatively high energy density, which makes it a promising material for biofuel production [20,21]. Saifuddin and Boyce [22] concluded that the properties of biodiesel produced from sunflower oil are within the ASTM (American Society for Testing and Materials) international standards. However, high viscosity remains a problem for its massive implementation. The production of biodiesel from blends of different types of raw material is one of the methods investigated to produce biodiesel with properties closer to conventional diesel.

Elkelawy et al. [23] investigated several blends of biodiesel produced from sunflower oil and soybean oil. The results indicated a decrease in CO and HC emissions and an increase in fuel consumption. Gupta et al. [24] investigated the optimization process for the production of biodiesel from blends of edible and inedible vegetable oils. The results show that the biodiesel obtained has good combustion properties that meet the ASTM standards. De Almeida et al. [25] studied the production of biodiesel from blends of residues of fish oil, palm oil, and frying oil. It was concluded that fuel properties, such as viscosity and oxidation stability, show improvements. The research developed by Costa et al. [26] showed that olive oil could be implemented to improve the properties of biodiesel produced from waste oils from the fishing industry.

The previous studies show the viability of the blends of different raw materials for the production of biodiesel, showing in some cases an improvement in the physical and chemical properties compared to the single use of a material. However, a large part of the biodiesel studies consisting of blends of different oils, do not show results from the analysis of this type of biodiesel in the combustion parameters and its relationship with polluting emissions.

The objective of this work is to evaluate the combustion, performance and emission characteristics of a diesel–biodiesel blend produced from two major polluting sources: residual sunflower oil and palm oil from agroindustry liquid waste because this two residues offer the highest production per

hectare of crop and have characteristics relatively close to conventional diesel compared to other sources of raw material. Therefore, a combustion diagnostic model based on the combustion chamber pressure has been developed in order to study the effect of the biofuel produced in the combustion processes of a single-cylinder diesel engine of low displacement, which is widely used in areas not interconnected for energy production. In addition, the effect of the combustion process on yield and CO, CO_2, NOx, and smoke opacity emissions are studied.

2. Diagnosis Model Description

In the diagnostic model in this paper, behavior in the combustion chamber of a single-cylinder diesel engine is assumed as an open system thermodynamic model. The above assumption is in accordance with previous studies in the literature [27,28]. The objective of the combustion model is to forecast the thermal efficiency of the engine based on the operating conditions of the engine, such as pressure, temperature, and mass inside the combustion chamber. With this, find the influence that these parameters have on emissions.

2.1. Diagnostic Model Considerations

The following are the main considerations for the formulation of the diagnostic model:

1. Uniform pressure inside the combustion chamber. This assumption is valid because the velocity of fluid propagation and the velocity of the combustion flame are much lower than the velocity of the sound [29].
2. The gases inside the combustion chamber have an ideal gas behavior. Valencia et al. [30] demonstrated the validity of this assumption in internal combustion engines.
3. The specific heat of the gases depends only on the chemical composition and temperature. This assumption is the result of the above consideration, as it is assumed to be a blend of ideal gases.
4. The combustion products are calculated stoichiometrically. This assumption is valid since most of the combustion process in the chamber of a diesel engine is diffusion combustion. Therefore, the consideration of stoichiometric combustion is valid [31].
5. Thermodynamic properties are calculated at the mean temperature of the combustion chamber. This assumption is valid since the phenomena of diffusion and heat transfer tend to stabilize the temperature uniformly inside the chamber.
6. Heat transfer through the cylinder walls and deformations of the piston mechanism are taken into consideration above to obtain results closer to the nature of the phenomenon.
7. Woschni's equations [32,33] are used to calculate the heat transfer coefficients.

2.2. Fundamental Equations of the Diagnostic Model

2.2.1. Engine Energy Balance

Equation (1) represents the thermodynamic model inside the combustion chamber. The model relates the variables of temperature, pressure, and mass inside the chamber as a function of the crankshaft angle.

$$\frac{dU}{d\theta} = \frac{dQ}{d\theta} - \frac{dW}{d\theta} + \sum_i \frac{dh_i}{d\theta} \quad (1)$$

where the subscript i is the input or output of the system.

Assuming an ideal gas behavior, Equation (1) can be expressed, as shown in Equation (2).

$$m_{comb} \cdot C_v \frac{dT}{d\theta} + u_f \frac{dm_f}{d\theta} = \frac{dQ_c}{d\theta} - \frac{dQ_r}{d\theta} - \frac{m_{comb} \cdot R_{comb} \cdot T}{V} \cdot \frac{dV}{d\theta} + \sum_i \left(h_i \cdot \frac{dm_{comb,i}}{d\theta}\right) \quad (2)$$

where Q_c and Q_r is the heat released from the chemical process during the combustion process and the transfer of heat through the cylinder walls.

The diagnostic model in this paper is based on the calculation of the heat release rate caused by the combustion process. Therefore, the calculation is made for the process release rate, based on Equations (2) and (3) shows the result obtained.

$$HRR = \frac{P \cdot \frac{dV}{d\theta} + m_{comb} \cdot C_v \cdot \frac{\Delta T}{\Delta \theta} + \frac{dQ_r}{d\theta} - \frac{dm_f}{d\theta} \cdot \left[h_{fl(T_{inj})} - u_f\right] + \frac{dm_{bb}}{d\theta} \cdot R_{comb} \cdot T}{m_{comb} \cdot LHV_f} \quad (3)$$

where each term indicates the following:

$P \cdot \frac{dV}{d\theta}$	Work is done inside the combustion chamber.
$m_{comb} \cdot C_v \cdot \frac{\Delta T}{\Delta \theta}$	Change of internal energy in the combustion chamber.
$\frac{dQ_r}{d\theta}$	Heat rejected by convection of the combustion chamber.
$\frac{dm_f}{d\theta} \cdot \left[h_{fl(T_{inj})} - u_f\right]$	Energy associated with fuel injection and vaporization.
$\frac{dm_{bb}}{d\theta} \cdot R_{comb} \cdot T$	Flow work associated with losses due to leaks in the combustion chamber.
$m_{comb} \cdot LHV_f$	It is the total energy generated by the fuel injected during the cycle.

The temperature (T) inside the combustion chamber is calculated with Equation (4).

$$T = \frac{P \cdot V}{m_{comb} \cdot R_{comb}} \quad (4)$$

where P, V, m_{comb} and R_{comb}, are mean combustion chamber pressure, combustion chamber volume, the mass of combustion chamber gas, and ideal gas constant, respectively.

2.2.2. Mass Balance in a Closed Cycle

When the piston is located between the bottom dead center and the top dead center, a fraction of the mass inside the combustion chamber escapes due to the intake valve delay. Therefore, the real mass in the combustion chamber is given by Equation (5).

$$m_{comb} = m_{IVC} + \int_{IVC}^{EVO} dm_f - \int_{IVC}^{EVO} dm_{bb} \quad (5)$$

where m_{IVC} is the mass trapped in the cylinder at IVC, $\int_{IVC}^{EVO} dm_f$ is all the mas of fuel injected (all injections are considered) and $\int_{IVC}^{EVO} dm_{bb}$ is all the blow-by leakages during this time frame.

2.2.3. Model of Gas Properties

The gas constant inside the combustion chamber is defined by Equation (6).

$$R_c = Y_a R_a + Y_b R_b + Y_f R_f \quad (6)$$

where R_c is the gas constant contained in the cylinder, R_a, R_b, R_f are the gas constants of the air, stoichiometric combustion products, and gaseous fuel. Y_a, Y_b, Y_f are the mass fractions of the air, stoichiometric combustion products, and the gaseous fuel, respectively.

2.2.4. Heat Transfer Model

The heat transfer rate produced between the combustion blend and the cylinder walls is shown in Equation (7).

$$\frac{dQ_r}{dt} = h_c \cdot A_w \cdot (T - T_w) \quad (7)$$

where h_c is the heat transfer coefficient, A_w is the heat transfer surface area of the combustion chamber, T is the average temperature of the gas inside the cylinder and T_w is the chamber wall temperature of combustion.

Equations (8) and (9) show the calculation of heat transfer coefficients.

$$h_c = C \cdot B^{m-1} \cdot P^m \cdot w^m \cdot T^{0.75-1.62m} \tag{8}$$

$$w = C_1 \cdot v_{mp} + C_2 \cdot \frac{V_{disp} \cdot T_{ref}}{P_{ref} \cdot V_{ref}} \cdot (P - P_r) \tag{9}$$

where B is the diameter of the hole, P is the pressure inside the combustion chamber, w is the average velocity of the gases inside the cylinder and P_r is the pressure of the combustion chamber if the engine was in a test. The constant C takes a value of 3.26, while the constant C_2 takes a value of 3.24×10^{-3} (during combustion) and zero (when no combustion is present), which is based on Woschni's research [33].

The constant C_1 is obtained by means of Equation (10).

$$C_1 = C_{W1} + C_{W2} \cdot \frac{v_{u\,(\theta)}}{v_{mp}} \tag{10}$$

where C_{W1} and C_{W2} are constants that depend on the stroke (compression, expansion, and admission) [33].

2.2.5. Combustion Chamber Volume Model

Equation (11) shows the instantaneous calculation of the combustion chamber volume with respect to the angular position of the crankshaft and considering volume variations due to pressure and inertia deformations [34].

$$V_{p,i}(\theta) = \frac{\pi \cdot D_4^2}{4} \cdot \left[\frac{2L_2}{(r_c - 1)} + L_2 + L_3 - R_{4y}(\theta) + \frac{K_{def}}{E_{steel} \cdot A_{CR}} \cdot L_3 \cdot \left(p_{gas} A_4 + m_i \cdot ac_4 \right) \right] \tag{11}$$

where K_{def} is the mechanical deformation constant that must be adjusted from experimental data. When considering cylinder clearances, Equation (11) is expressed as [34]:

$$\begin{aligned} V(\theta) \quad = \frac{\pi \cdot D_4^2}{4} \cdot \Bigg[& \frac{2L_2}{(r_c - 1)} + L_2 + L_3 - R_{4y}(\theta) + \frac{K_{def}}{E_{steel} \cdot A_{CR}} \cdot L_3 \cdot \left[p_{gas} A_4 + m_i \cdot ac_4 \right] \\ & + \sum_{i=1}^{2} -e_i \cdot \sin(\gamma_i) \cdot \cos(\beta_i) \Bigg] \end{aligned} \tag{12}$$

2.2.6. Blow-By Losses

The losses due to gas leaks inside the combustion chamber are calculated using Equation (13). This equation is based on the approximations proposed by Irimescu [35].

$$dm_{bb} = A_{bb} \cdot \rho \cdot \sqrt{2 \cdot \frac{\gamma}{\gamma - 1} \cdot \frac{R}{M \cdot T} \cdot \left[1 - \left(\frac{p_0}{p} \right)^{\frac{\gamma - 1}{\gamma}} \right]} \tag{13}$$

where A_{bb} is the equivalent blow-by, ρ gas density, γ ratio of specific heat capacities, R universal gas constant, M molar mass, and p_0 ambient pressure.

3. Diagnostic Model Procedure

Figure 1 shows a general procedure for the diagnosis of a diesel engine. The procedure begins with the acquisition of the experimental pressure signal and the position of the crankshaft angle, using

piezoelectric transducers and optical encoders. This signal is then processed through the average of cycles and low pass filters. The cylinder pressure and volume function obtained from the data processing is used to calculate the instantaneous average combustion gas temperature in the chamber. After calculating the thermodynamic properties of the gas, the heat transfer, and the heat release law, the corresponding curves of heat release rate and cumulative heat release are obtained.

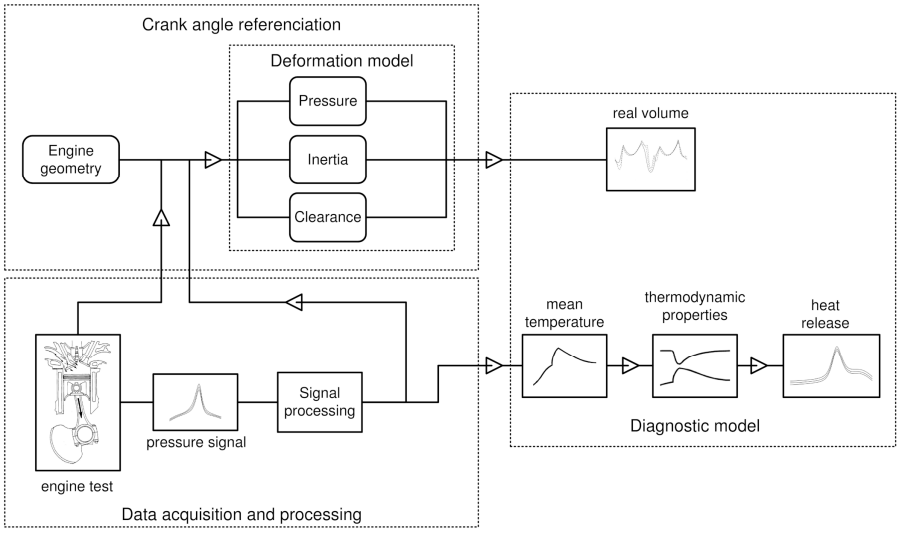

Figure 1. General scheme of the diagnostic model.

The flow diagram of the diagnostic model proposed in this paper can be seen in Figure 2. This figure shows the schema of the mathematical model described in Section 2.

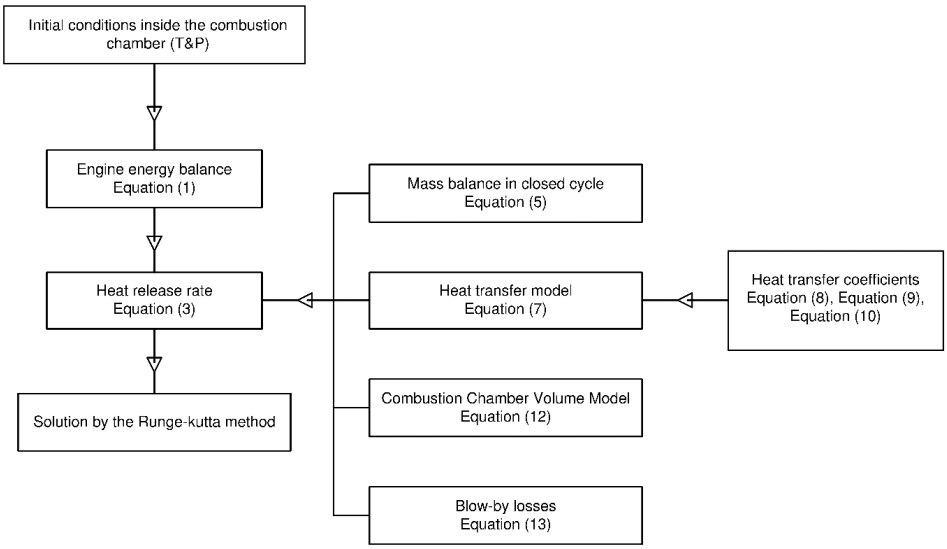

Figure 2. Flow chart of the diagnostic model.

4. Experimental Setup and Procedure

4.1. Experimental Instruments

For the experimental test, a stationary diesel engine, single-cylinder, four strokes, and natural aspiration was used. Detailed engine features are shown in Table 1.

Table 1. Specifications of the diesel engine.

Model	SK-MDF300
Engine type	1 cylinder
Manufacturer	SOKAN
Cycle	4 Strokes
Bore × stroke	78 mm × 62.57 mm
Displaced volume	299 CC
Compression ratio	20:1
Maximum power	4.6 hp at 3600 rpm
Intake system	Naturally Aspirated
Injection system	Direct injection
Injection Angle	20° BTDC

The engine is coupled to a dynamometer to apply different loading conditions. A crankshaft angle sensor, Beck Arnley 180-0420, was used in the engine to measure its rotation speed. To measure the pressure inside the cylinder, a KISTLER type 7063-A piezoelectric sensor is installed in the cylinder head. The fuel consumption rate was measured using a gravimetric meter OHAUS PA313, and a stopwatch, the measurement of the gravimetric meter was taken at the beginning and end of the experiment, and with the use of the stopwatch, the duration of the test was measured. The measurement of the intake air flow is performed using a BOSCH 22680 7J600 hot wire meter. To measure the high temperatures of the flue gases, K-type thermocouples were used. For the measurement of emissions, the BrainBee AGS-688 and PCA® 400 gas analyzers were used to measure the levels of CO, CO_2, NOx, and HC. Additionally, the opacity levels of the exhaust gases were measured with the BrainBee OPA-100 opacimeter. All measuring instruments are connected to a computer through a data acquisition system.

The diagram of the experimental test bench is shown in Figure 3. The measuring range and accuracy of the measuring instruments are shown in Table 2.

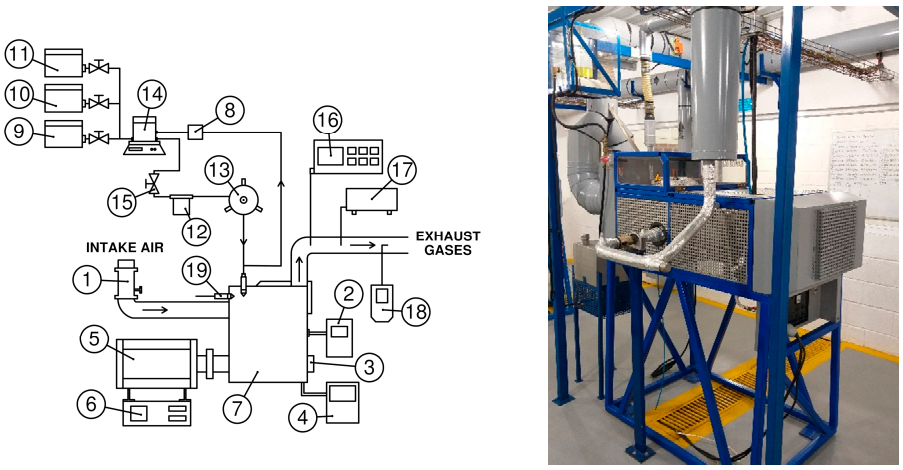

(**a**) (**b**)

1. Air flow meter, 2. Data acquisition (DAQ), 3. Crank angle encoder, 4. Median variables DAQ, 5. Dynamometer, 6. Resistive test bench, 7. Test engine, 8. Pressure regulator, 9. Diesel tank, 10. PB tank, 11. SB tank, 12. Fuel filter, 13. Injection pump, 14. Gravimetric fuel meter, 15. Fuel inlet valve, 16. BrainBee AGS-688 Emission gas, 17. Opacimeter, 18. PCA® 400 Emission gas analyzer, 19. Piezoelectric transducer.

Figure 3. Engine test bench, (**a**) setup, and (**b**) devices.

Table 2. Specifications of measuring instruments.

Measuring Instrument	Manufacturer	Range		Accuracy
Thermocouple	Type K	−200–1370 °C		0.1%
Piezoelectric transducer	KISTLER type 7063-A	0–250 bar		<±0.5%
Gravimetric meter	OHAUS PA313	0–310 g		1%
Hot wire	BOSCH 22680 7J600	0–125 g/s		1%
Hall effect	NJK-5002C	5–9999 RPM		0.03%
Exhaust gas analyzer	BrainBee AGS-688	CO	0 ÷ 9.99 vol%	±0.1%
		CO_2	0 ÷ 19.9 vol%	±0.01%
		HC	0 ÷ 19.999 ppm	±1%
	PCA® 400	NOx	0 ÷ 3000 ppm	±0.5%
Smoke meter	BrainBee OPA-100	0 ÷ 99.9%		±0.1%

4.2. Test Conditions and Fuels

Diesel fuel and biodiesel blends produced from palm oil from agro-industrial liquid waste and residual sunflower oil were used in this study. In total, five types of designated fuels were investigated, as shown in Table 3.

Table 3. Nomenclature and composition of fuels.

Nomenclature	Composition
D100	Diesel 100%
PB5	Diesel 95% + Palm oil biodiesel 5%
PB10	Diesel 90% + Palm oil biodiesel 10%
PB5SB5	Diesel 90% + Palm oil biodiesel 5% + Sunflower oil biodiesel 5%
PB10SB5	Diesel 85% + Palm oil biodiesel 10% + Sunflower oil biodiesel 5%

The percentage of biodiesel from palm oil remained up to 10%, due to national legislative standards. In general, the percentage of diesel replacement remained below 20% since research shows that below 20% biodiesel has no negative effect on the engine, and the properties of fuels remain relatively close to diesel [36–38]. The properties of diesel and biodiesel blends were measured in a Test Laboratory, following the use of the US ASTM standard tests. The properties of these fuels are shown in Table 4.

Table 4. Physicochemical properties of the fuels.

Property	Units	Standards	D100	PB5	PB10	PB5SB5	PB10SB5
Density	kg/m^3	ASTM D1298	821.5	823.1	827.5	829.1	833
Viscosity	cSt	ASTM D445	2.64	2.65	2.66	2.68	2.69
Flash point	°C	ASTM D93	76	85	96	98	100
Cloud point	°C	ASTM D2500	6.5	7.2	8.3	8.5	9.1
Pour point	°C	ASTM D97	3.1	3.5	3.8	4	4.3
NCP	MJ/kg	ASTM D240	44.05	43.89	43.25	42.28	41.67

In the experimental process, four different engine operating conditions A, B, C, and D were tested. The characteristics of each of these conditions are shown in Figure 4.

These conditions were selected to evaluate the main conditions of engine operation. In addition, the difference between conditions A and B with C and D allows the creation of extreme conditions of pressure, temperature, and fuel flow, which allows the combustion processes of the engine to be studied in a wide range.

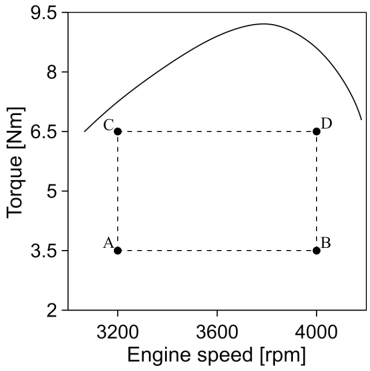

Figure 4. Engine operating conditions.

5. Results and Discussion

5.1. Combustion Characteristics

5.1.1. Cylinder Pressure

Cylinder pressure is an indication of fuel efficiency and the ability to mix air with fuel. Figure 5 shows the change in pressure in the cylinder for diesel and biodiesel blends. It was observed that the maximum pressure reached was 56.5, 63.28, 67.8, and 72.32 bar for operating modes A, B, C, and D. In all operating modes, diesel generated the maximum pressures. This behavior is consistent with similar studies [39].

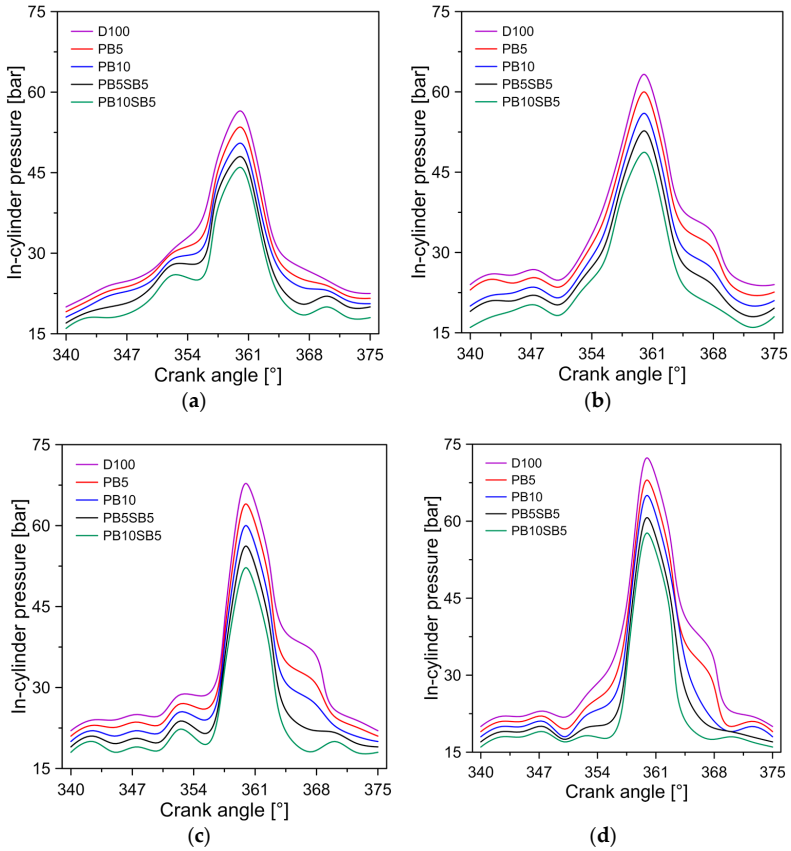

Figure 5. Influence of fuel on cylinder pressure for (**a**) mode A, (**b**) mode B, (**c**) mode C, and (**d**) mode D.

The blends of biodiesel PB5 and PB10 showed a decrease in chamber pressure of 5.1% and 9.8%, compared to diesel, respectively. Similarly, blends of biodiesel PB5SB5 and PB10SB5 showed a decrease in in-cylinder pressure of 12% and 15.6%, compared to diesel, respectively. The greater pressure reduction in biodiesel with sunflower blends is attributed to the lower calorific value of this biodiesel, as shown in Table 4. Musthafa et al. [40] study present a similar behavior with other types of biodiesel.

5.1.2. Heat Release Rate (HRR)

The HRR indicates the chemical energy of the fuel that is converted into thermal energy. Figure 6 shows the variation of HRR with respect to the angle of the crankshaft for diesel and biodiesel blends. In general, diesel has the highest HRRs for the modes of operation tested, followed by PB5, PB10, PB5SB5, and PB10SB5, respectively. It was observed that the maximum HRR was 1.08, 1.14, 1.18, 1.22, and 1.26 J/deg for PB10SB5, PB5SB5, PB10, PB5, and diesel in the mode of operation D, respectively. On average, the HRRs of PB5SB5 and PB10SB5 decreased by 3.38% and 8.47% compared to PB10 biodiesel. Viscosity is considered the key factor for this behavior because it produces slower combustion, resulting in a reduction in heat release. Similar behavior was obtained in the investigation of Can [41].

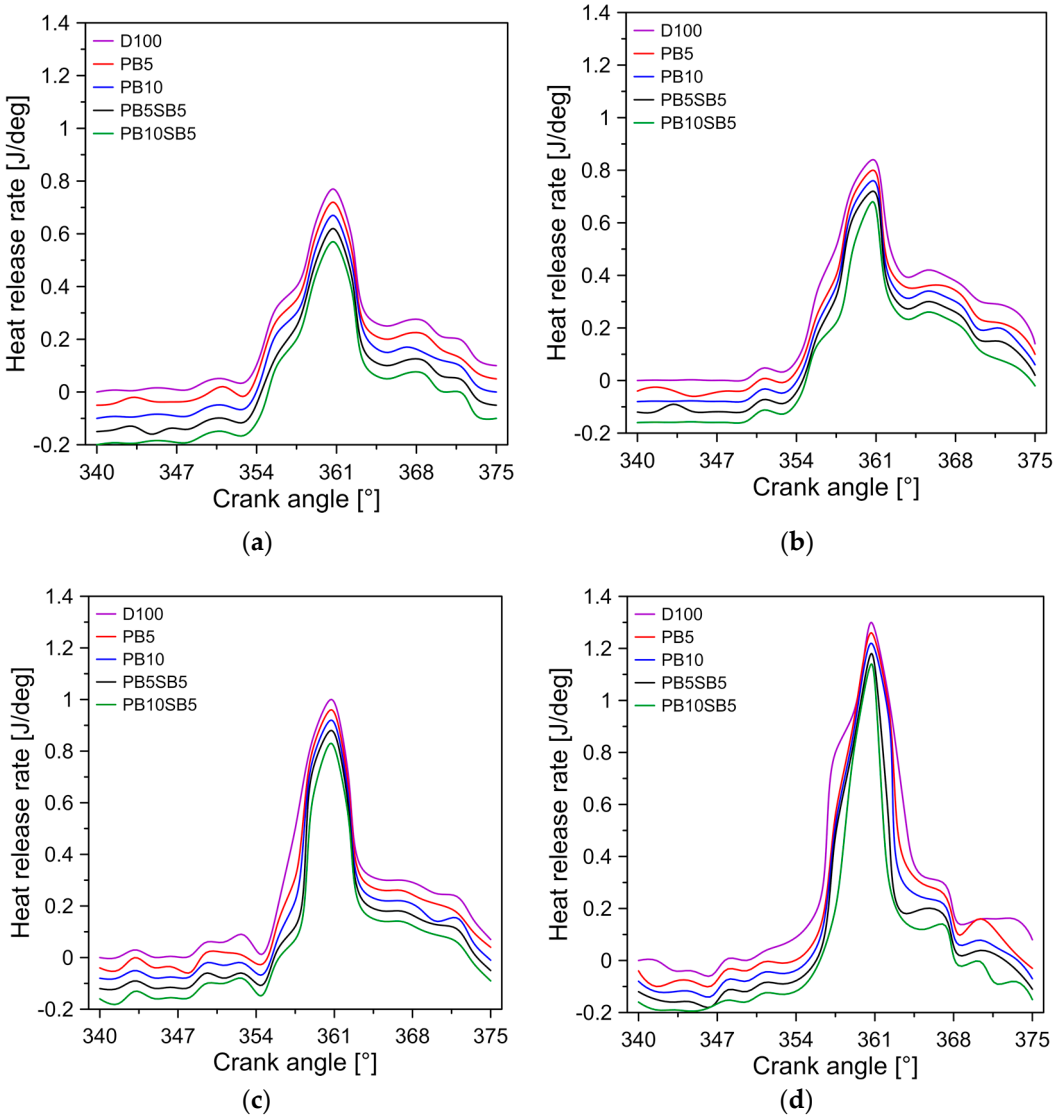

Figure 6. Influence of fuel on heat release rate for (**a**) mode A, (**b**) mode B, (**c**) mode C, and (**d**) mode D.

5.1.3. Cumulative Heat Release Rate

Figure 7 shows the release of accumulated heat with respect to the angle of the crankshaft for the four modes of operation and the three fuels. In all modes of operation, it was observed that biodiesel blends have a higher cumulative heat release compared to diesel. This indicates that biodiesel blends are less efficient in converting thermal energy into mechanical energy. In general, PB10SB5, PB5SB5, PB10, and PB5 show an increase in the cumulative release rate of 13.9%, 12.98%, 7.45%, and 6.92% compared to diesel, respectively.

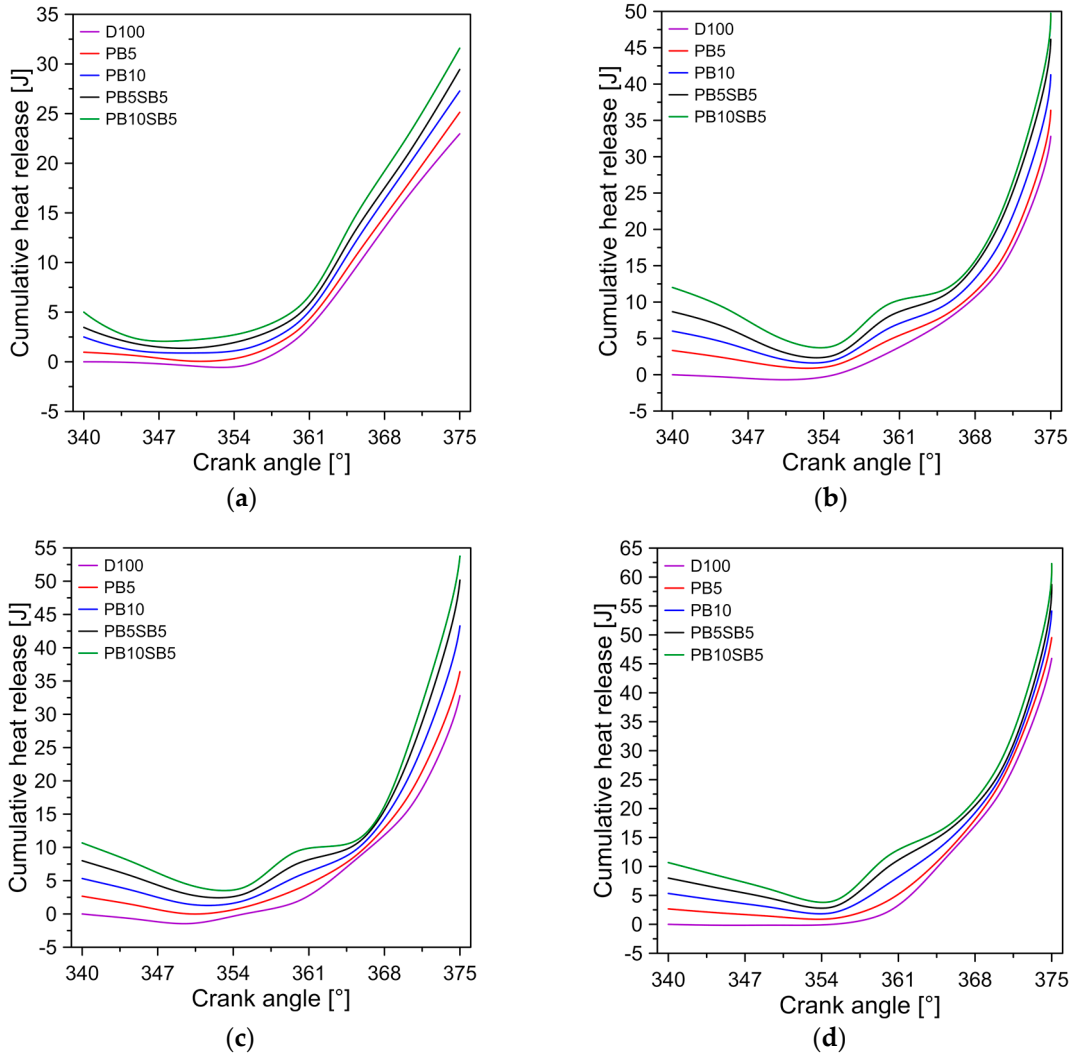

Figure 7. Accumulated heat rate diagram for (**a**) mode A, (**b**) mode B, (**c**) mode C, and (**d**) mode D.

5.1.4. Combustion Chamber Temperature

Figure 8 shows the average temperature of the cylinder chamber for the five fuels tested. In general, biodiesel blends with sunflower oil content have higher temperatures than palm oil biodiesel and diesel. On average, the combustion chamber temperature of the PB5SB5 and PB10SB5 is increased by 6.21% and 12.23% compared to palm oil biodiesel and diesel. This behavior is due to the increased presence of oxygen in sunflower oil, which improves the combustion process and increases the temperature of the cylinder chamber. Similar behavior is reported by Dueso et al. [42].

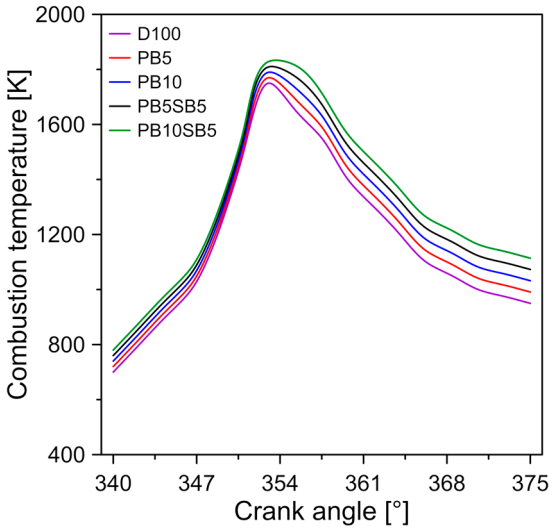

Figure 8. In-cylinder temperature in mode D.

5.2. Engine Performance

Figure 9a shows the effect of biodiesel blends on the specific fuel consumption and thermal efficiency of the engine with respect to the engine's mode of operation. In general, the increase in the percentage of biodiesel causes an increase in specific fuel consumption. It was observed that on average, the PB10SB5, PB5SB5, PB10, and PB5 show an increase in specific fuel consumption of 13.28%, 11.48%, 7.64%, and 3.8% compared to diesel, respectively. The cause of this behavior is mainly due to the lower calorific value of biodiesel blends. Therefore, a greater amount of fuel is needed to reach the same amount of power. Additionally, it is observed that biodiesel blends have a higher density and viscosity than diesel, so the amount of fuel injected into the combustion chamber is greater [43,44].

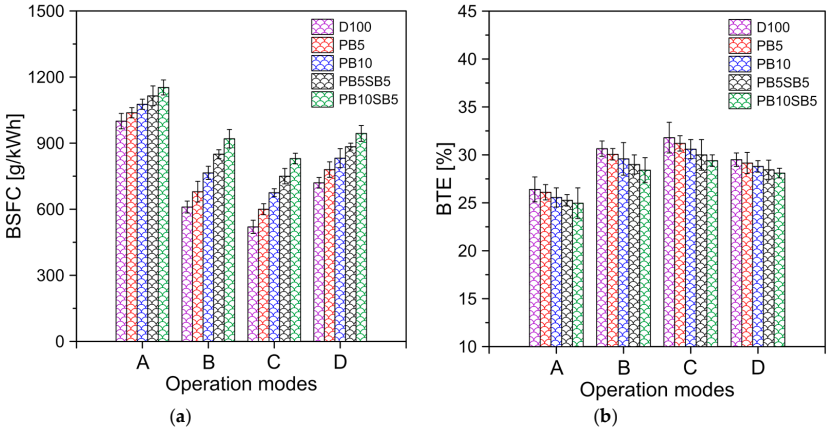

Figure 9. Diagram of (**a**) specific fuel consumption, and (**b**) brake thermal efficiency.

In addition, it was observed that an increase in engine load causes a reduction in the BSFC (Brake-specific fuel consumption) value because the combustion process is more efficient with higher loads. Similar results were reported in the investigations of Ozener et al. [45], and Emiroğlu and Şen [46].

The thermal efficiency of the brake (BTE) is a parameter that measures the combustion capacity of the fuel to transform its chemical energy into mechanical energy. The BTE against the different engine loads is shown in Figure 9b. The addition of biodiesel is reflected in the efficiency of the thermal brake. It was observed that biodiesel blends show a reduction in the thermal efficiency of the brake. For the different modes analyzed, it is shown that the BTE varies from 26.4–31.8%, 26.1–31.2%, 25.56–30.6%,

25.26–30% and 24.96–29.4% for diesel, PB5, PB10, PB5SB5, and PB10SB5, respectively. This efficiency reduction can be explained by the higher fuel consumption and the lower calorific value of biodiesel blends, as shown in Table 4.

5.3. Emission Characteristics

To analyze the effect of combustion parameters on emission characteristics, CO, CO_2, HC, NOx, and smoke opacity emissions were measured for the four modes of operation.

5.3.1. CO and CO_2 Emissions

Carbon monoxide (CO) emissions with respect to engine operation mode are shown in Figure 10a. It was observed that at low load levels, CO emissions are higher compared to the operation of the engine at full load. This behavior is due to the fact that at higher load levels, the engine runs more efficiently, which requires less fuel to reach working power. Biodiesel blends produced lower emissions than diesel fuel. In general, the CO emissions of PB5, PB10, PB5SB5, and PB10SB5 were 14%, 23%, 26%, and 28% lower compared to diesel, respectively. This is due to the higher oxygen content of biodiesel, which produces complete combustion and, therefore, lower CO emissions.

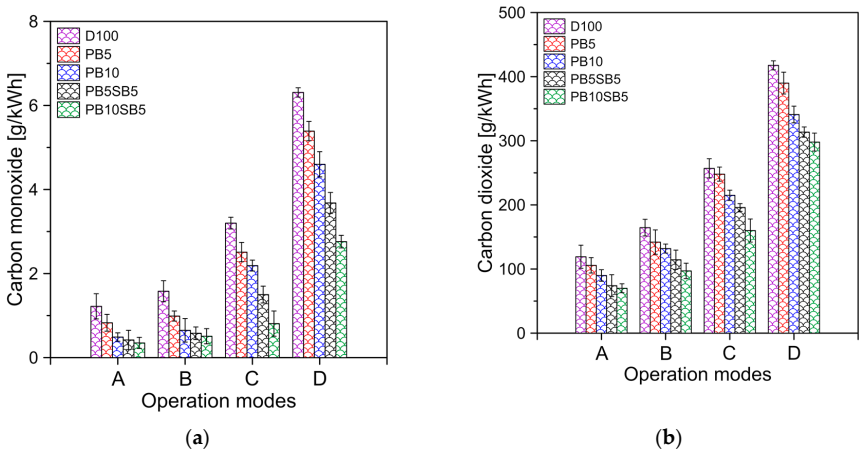

Figure 10. (**a**) CO and (**b**) CO_2 emissions for fuels tested.

Figure 10b shows the carbon dioxide (CO_2) emissions with respect to the mode of operation of the engine. It is observed again that the increase in the percentage of biodiesel allows the reduction of CO_2 emissions. As with CO emissions, biodiesel blends with sunflower oil percentage had lower emissions than biodiesel blends with palm oil alone. On average, the blends of PB5SB5 and PB10SB5 showed a 20% greater reduction than the blends PB5 and PB10, respectively. The greater presence of oxygen in the biodiesel PB5SB5 and PB10SB5 causes a cleaner and complete combustion process. Similar results can be seen in the references [47,48].

5.3.2. NOx and HC Emissions

The formation of NOx depends largely on the temperature inside the cylinder, the concentration of oxygen in the fuel, and the residence time of the reaction. Figure 11a shows the emissions of nitrogen oxides (NOx) for all test fuels. Higher NOx formations were produced by increasing the percentage of biodiesel in the fuel. Blends with sunflower oil PB5SB5 and PB10SB5 had the highest NOx emission rates. On average, it was observed that biodiesel PB5, PB10, PB5SB5, and PB5SB10 produce 5.46%, 9.81%, 14.32%, and 18.3% more NOx emissions compared to diesel, respectively. The above results can be explained by considering the greater presence of oxygen in the biodiesel blends, mainly in the PB5SB5 and PB10SB5, and the higher temperatures reached by the biodiesel, as shown in Figure 8.

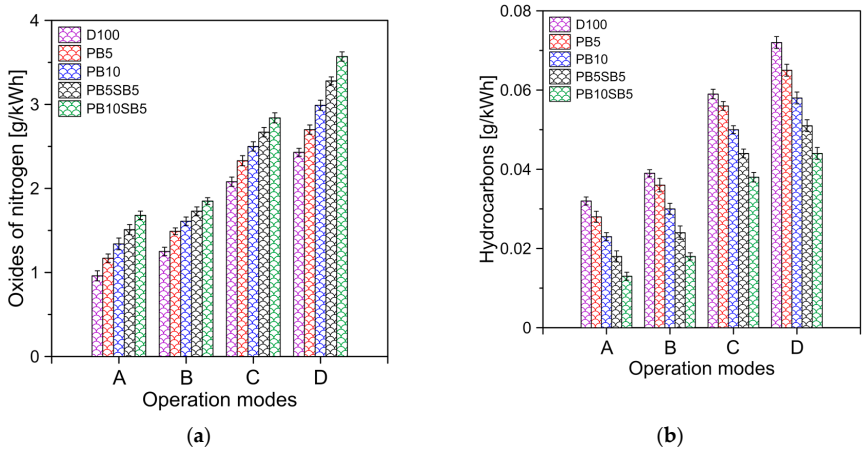

Figure 11. (**a**) NOx and (**b**) HC, emissions for fuels tested.

Figure 11b shows the variation of HC emissions with respect to engine operating modes. HC emissions decrease with the increase in the percentage of biodiesel in the fuel. Hydrocarbons are the product of incomplete combustion of fuel. Therefore, more efficient combustion allows for reducing this type of emissions. In this case, the oxygen content of the biodiesel blends allows the combustion process to be improved. Therefore, it results in a lower amount of hydrocarbon emissions. On average, the HC emissions for PB5, PB10, PB5SB5, and PB10SB5 were 4.8%, 9.72%, 15.58% and 19.5% lower compared to diesel, respectively.

5.3.3. Smoke Emissions

The variation in the opacity of the smoke for the different fuels is shown in Figure 12. It was observed that the density of the smoke increases with the increases in the engine load since the smoke depends largely on the engine power. HC emissions were reduced by increasing the percentage of biodiesel in the fuel. It was observed that the minimum and maximum smoke density produced was 1.88–16.06 HSU, 2–19.04 HSU, 2.12–22.02 HSU, 4.21–25 HSU, 5.69–27.98 HSU for PB10SB5, PB5SB5, PB10, PB5, and diesel, respectively.

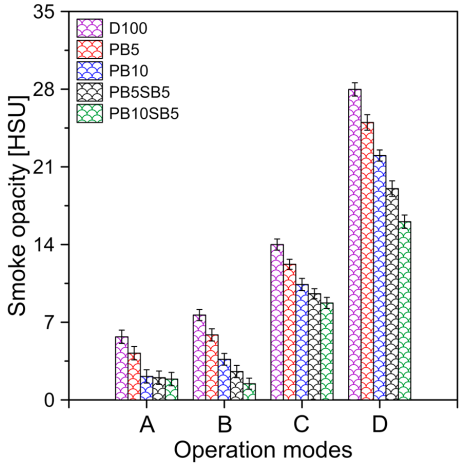

Figure 12. Smoke emissions for fuels tested.

The reduction in HC emissions is mainly due to oxygen molecules in the chemical structure of the fuel, which produces complete combustion inside the chamber [23]. Due to this fact, biodiesel with the percentage of sunflower oil has the lowest HC emissions, since its oxygen content is higher compared to palm oil blends.

6. Conclusions

In the present study, an analysis of the combustion process, performance, and emissions of a single-cylinder engine was carried out, using biodiesel blends formed by the blend of palm oil and sunflower oil residues.

The results of the diagnostic model show that the pressure curves in the cylinder chamber decrease as the biodiesel content in the fuel increases. For the modes of operation considered, the maximum pressures were found in the range of 16–57.58 bar, 17–60.68 bar, 18.1–65 bar, 19.1–68 bar and 20–72.32 bar for the PB10SB5, PB5SB5, PB10, PB5, and diesel, respectively. This decrease in pressure was attributed to the lower calorific value of biodiesel compared to diesel. Similarly, the results showed a decrease in the rate of heat release for biodiesel blends compared to diesel for all tested modes of operation. It was observed that in the highest engine operating mode, the HRR curves showed a maximum of 1.14 J/deg, 1.18 J/deg, 1.22 J/deg, 1.26 J/deg and 1.30 J/deg for the PB10SB5, PB5SB5, PB10, PB5, and diesel, respectively. The higher viscosity and lower calorific value of biodiesel blends are considered to cause this behavior. However, the addition of a percentage of sunflower oil residues does not cause a large difference in maximum pressures, and heat release rates, when compared to biodiesel produced only with residual palm oil.

The higher viscosity of the biodiesel tested also causes a reduction in the combustion rate, decreasing the heat release of the combustion process. This fact is reflected in the accumulated heat release curves, which were larger for fuels with a higher biodiesel content. This effect is reflected in the thermal efficiency of biodiesel blends. It was observed that the maximum thermal efficiency was 29.4%, 30%, 30.6%, 31.2% and 31.8% for PB10SB5, PB5SB5, PB10, PB5, and diesel, respectively.

The addition of the percentage of residual sunflower oil in biodiesel caused an increase in BSFC. On average, the PB10SB5 and PB5SB5 biodiesel increased the BSFC by 15.5% compared to the PB10 and PB5 biodiesel, respectively.

The emissions analysis showed that PB10SB5 and PB5SB5 fuels show a reduction in CO, CO_2, HC, and smoke opacity emissions of approximately 14–23%, 23.3–28.1%, 15.58–19.5% and 7.9–9.4% in comparison with pure diesel, respectively. The above-mentioned results are mainly attributed to the higher oxygen content in this type of biodiesel, contributing to a cleaner and complete combustion.

The temperature values in the combustion chamber showed that the addition of sunflower oil residues causes a rise in the maximum temperature. This temperature increase facilitated the production of NOx emissions. The results show that on average, the PB5SB5 and PB10SB5 increase NOx emissions by 8.3% compared to biodiesel blends of residual palm oil.

In general, biodiesel with the percentage of residual sunflower oil does not cause a significant change in the combustion process and engine performance, when compared to biodiesel that includes only residual palm oil. Despite the increase in NOx emissions, biodiesel blends with the addition of residual sunflower oil allow CO, CO_2, HC, and smoke opacity emissions to be reduced. Therefore, biodiesel produced by mixing palm oil and sunflower oil residues could be used to replace up to 15% diesel, allowing the reduction of highly polluting waste and the production of a cleaner and more renewable fuel.

Author Contributions: All the authors of the present research contributed equally to conducting and writing this paper. All authors have read and agreed to the published version of the manuscript.

Funding: This research received no external funding.

Acknowledgments: Acknowledgments to Universidad del Atlántico, Universidad Francisco de Paula Santander, to Sphere Energy Company and Colombian Institute for Scientific and Technological Development (COLCIENCIAS) through the "Convocatoria Nacional para Estudios de Doctorado en Colombia año 2012" for the support provided.

Conflicts of Interest: The authors declare no conflict of interest.

Abbreviations

The following abbreviations are used in this manuscript:

LHV_{fuel}	Lower heating value of fuel
HRR	Heat release rate
IVC	Inlet valve close
EVO	Exhaust valve open
BSFC	Brake specific fuel consumption
BTE	Brake thermal efficiency
B5	5% biodiesel blend
B10	10% biodiesel blend
CO	Carbon monoxide
CO_2	Carbon dioxide
NOx	Nitrogen oxides
HC	Hydrocarbons
HSU	Hartridge Smoke Unit
Nomenclature	
P	Mean combustion chamber pressure
V	Combustion chamber volume
m	Gas mass
C_v	Specific heat at constant volume
T	Combustion chamber gas temperature
Q	Heat release
Q_r	Heat rejected by convection
Q_c	Heat release during the combustion process
h	Specific enthalpy
R	Ideal gas constant
U	Internal energy
u	Specific Internal Energy
Y	Gas Mass Fraction
A_W	Heat transfer surface area of the combustion chamber
D	Diameter
L	Length
r_c	Compression ratio
K_{def}	Deformation constant
R_{4y}	Vertical position of the piston
E_{steel}	Elastic modulus of steel
A	Area
A_{CR}	Connecting rod's critical area
ac	Acceleration
e	Eccentricity between the stump and the bearing, located in its center line
M	Gas molecular weight
Greek Letters	
θ	Crankshaft angle
ρ	Fluid density
Subscripts	
4	Piston
comb	Combustion chamber gas
a	Air
b	Combustion Products
f	Fuel
fl	Liquid fuel
W	Combustion Chamber Wall
bb	Blow-by
inj	Injection
i	Inertial loads

References

1. Yoo, H.; Park, B.Y.; Cho, H.; Park, J. Performance Optimization of a Diesel Engine with a Two-Stage Turbocharging System and Dual-Loop EGR Using Multi-Objective Pareto Optimization Based on Diesel Cycle Simulation. *Energies* **2019**, *12*, 4223. [CrossRef]
2. Tian, H.; Cui, J.; Yang, T.; Fu, Y.; Tian, J.; Long, W. Experimental Research on Controllability and Emissions of Jet-Controlled Compression Ignition Engine. *Energies* **2019**, *12*, 2936. [CrossRef]
3. Dhar, A.; Agarwal, A.K. Effect of Karanja biodiesel blend on engine wear in a diesel engine. *Fuel* **2014**, *134*, 81–89. [CrossRef]
4. Hirner, F.S.; Hwang, J.; Bae, C.; Patel, C.; Gupta, T.; Agarwal, A.K. Performance and emission evaluation of a small-bore biodiesel compression-ignition engine. *Energy* **2019**, *183*, 971–982. [CrossRef]
5. Kumar, N.; Varun, G.; Chauhan, S.R. Performance and emission characteristics of biodiesel from different origins: A review. *Renew. Sustain. Energy Rev.* **2013**, *21*, 633–658. [CrossRef]
6. Zahan, K.; Kano, M. Biodiesel Production from Palm Oil, Its By-Products, and Mill Effluent: A Review. *Energies* **2018**, *11*. [CrossRef]
7. Bari, S.; Hossain, S.N. Performance and emission analysis of a diesel engine running on palm oil diesel (POD). *Energy Procedia* **2019**, *160*, 92–99. [CrossRef]
8. Sajjadi, B.; Raman, A.A.A.; Arandiyan, H. A comprehensive review on properties of edible and non-edible vegetable oil-based biodiesel: Composition, specifications and prediction models. *Renew. Sustain. Energy Rev.* **2016**, *63*, 62–92. [CrossRef]
9. Berchmans, H.J.; Hirata, S. Biodiesel production from crude Jatropha curcas L. seed oil with a high content of free fatty acids. *Bioresour. Technol.* **2008**, *99*, 1716–1721. [CrossRef]
10. Thushari, P.G.I.; Babel, S. Biodiesel Production From Waste Palm Oil Using Palm Empty Fruit Bunch-Derived Novel Carbon Acid Catalyst. *J. Energy Resour. Technol.* **2018**, *140*, 1–10. [CrossRef]
11. Sumathi, S.; Chai, S.P.; Mohamed, A.R. Utilization of oil palm as a source of renewable energy in Malaysia. *Renew. Sustain. Energy Rev.* **2008**, *12*, 2404–2421. [CrossRef]
12. Kurnia, J.C.; Jangam, S.V.; Akhtar, S.; Sasmito, A.P.; Mujumdar, A.S. Advances in biofuel production from oil palm and palm oil processing wastes: A review. *Biofuel Res. J.* **2016**, *3*, 332–346. [CrossRef]
13. Sulaiman, S.A.; Taha, F.F.F. Drying of Oil Palm Fronds Using Concentrated Solar Thermal Power. *Appl. Mech. Mater.* **2014**, *699*, 449–454. [CrossRef]
14. Lam, S.S.; Tsang, Y.F.; Yek, P.N.Y.; Liew, R.K.; Osman, M.S.; Peng, W.; Lee, W.H.; Park, Y.-K. Co-processing of oil palm waste and waste oil via microwave co-torrefaction: A waste reduction approach for producing solid fuel product with improved properties. *Process Saf. Environ. Prot.* **2019**, *128*, 30–35. [CrossRef]
15. Cho, H.J.; Kim, J.-K.; Cho, H.-J.; Yeo, Y.-K. Techno-Economic Study of a Biodiesel Production from Palm Fatty Acid Distillate. *Ind. Eng. Chem. Res.* **2012**, *52*, 462–468. [CrossRef]
16. Liew, W.; Muda, K.; Azraai, M.; Affam, A.; Loh, S. Agro-industrial waste sustainable management–a potential source of economic benefits to palm oil mills in Malaysia. *J. Urban Environ. Eng.* **2017**, *11*, 108–118. [CrossRef]
17. Ahmad Farid, M.A.; Hassan, M.A.; Taufiq-Yap, Y.H.; Ibrahim, M.L.; Othman, M.R.; Ali, A.A.M.; Shirai, Y. Production of methyl esters from waste cooking oil using a heterogeneous biomass-based catalyst. *Renew. Energy.* **2017**, *114*, 638–643. [CrossRef]
18. Anuar, M.R.; Abdullah, A.Z. Ultrasound-assisted biodiesel production from waste cooking oil using hydrotalcite prepared by combustion method as catalyst. *Appl. Catal. A Gen.* **2016**, *514*, 214–223. [CrossRef]
19. Hong, I.K.; Jeon, H.; Kim, H.; Lee, S.B. Preparation of waste cooking oil based biodiesel using microwave irradiation energy. *J. Ind. Eng. Chem.* **2016**, *42*, 107–112. [CrossRef]
20. Ramírez, R.; Gutiérrez, A.S.; Eras, J.J.C.; Valencia, K.; Hernández, B.; Forero, J.D. Evaluation of the energy recovery potential of thermoelectric generators in diesel engines. *J. Clean. Prod.* **2019**, *241*, 118412. [CrossRef]
21. Saydut, A.; Kafadar, A.B.; Tonbul, Y.; Kaya, C.; Aydin, F.; Hamamci, C. Comparison of the Biodiesel Quality Produced from Refined Sunflower (Helianthus Annuus L) Oil and Waste Cooking Oil. *Energy Explor. Exploit.* **2010**, *28*, 499–512. [CrossRef]
22. Saifuddin, M.; Boyce, A.N. Biodiesel production from waste cooking sunflower oil and environmental impact analysis. *Kuwait J. Sci.* **2016**, *43*, 110–117.

23. Elkelawy, M.; Alm-Eldin Bastawissi, H.; Esmaeil, K.K.; Radwan, A.M.; Panchal, H.; Sadasivuni, K.K.; Ponnamma, D.; Walvekar, R. Experimental studies on the biodiesel production parameters optimization of sunflower and soybean oil mixture and DI engine combustion, performance, and emission analysis fueled with diesel/biodiesel blends. *Fuel* **2019**, *255*. [CrossRef]
24. Gupta, J.; Agarwal, M.; Dalai, A.K. Optimization of biodiesel production from mixture of edible and nonedible vegetable oils. *Biocatal. Agric. Biotechnol.* **2016**, *8*, 112–120. [CrossRef]
25. De Almeida, V.F.; García-Moreno, P.J.; Guadix, A.; Guadix, E.M. Biodiesel production from mixtures of waste fish oil, palm oil and waste frying oil: Optimization of fuel properties. *Fuel Process. Technol.* **2015**, *133*, 152–160. [CrossRef]
26. Costa, J.F.; Almeida, M.F.; Alvim-Ferraz, M.C.M.; Dias, J.M. Biodiesel production using oil from fish canning industry wastes. *Energy Convers. Manag.* **2013**, *74*, 17–23. [CrossRef]
27. Valencia, G.; Núñez, J.; Duarte, J. Multiobjective optimization of a plate heat exchanger in a waste heat recovery organic rankine cycle system for natural gas engines. *Entropy* **2019**, *21*. [CrossRef]
28. Diaz, G.A.; Forero, J.D.; Garcia, J.; Rincon, A.; Fontalvo, A.; Bula, A.; Padilla, R.V. Maximum Power From Fluid Flow by Applying the First and Second Laws of Thermodynamics. *J. Energy Resour. Technol.* **2017**, *139*. [CrossRef]
29. Ochoa, G.V.; Isaza-Roldan, C.; Forero, J.D. A phenomenological base semi-physical thermodynamic model for the cylinder and exhaust manifold of a natural gas 2-megawatt four-stroke internal combustion engine. *Heliyon* **2019**, *5*, e02700. [CrossRef]
30. Valencia Ochoa, G.; Acevedo Peñaloza, C.; Duarte Forero, J. Thermoeconomic optimization with PSO Algorithm of waste heat recovery systems based on Organic Rankine Cycle system for a natural gas engine. *Energies* **2019**, *12*, 4165. [CrossRef]
31. Glassman, I. *Combustion*; Academic Press Inc.: Cambridge, MA, USA, 1987.
32. Woschni, G. A Universally Applicable Equation for the Instantaneous Heat Transfer Coefficient in the Internal Combustion Engine. *SAE Tech. Pap.* **1967**. [CrossRef]
33. Woschni, G. Die berechnung der wandverluste und der thermischen belastung der bauteile von dieselmotoren. *MTZ Mot. Z.* **1970**, *31*, S491–S499.
34. Consuegra, F.; Bula, A.; Guillín, W.; Sánchez, J.; Duarte Forero, J. Instantaneous in-Cylinder Volume Considering Deformation and Clearance due to Lubricating Film in Reciprocating Internal Combustion Engines. *Energies* **2019**, *12*. [CrossRef]
35. Irimescu, A.; Di Iorio, S.; Merola, S.S.; Sementa, P.; Vaglieco, B.M. Evaluation of compression ratio and blow-by rates for spark ignition engines based on in-cylinder pressure trace analysis. *Energy Convers. Manag.* **2018**, *162*, 98–108. [CrossRef]
36. Alptekin, E.; Canakci, M. Characterization of the key fuel properties of methyl ester–diesel fuel blends. *Fuel* **2009**, *88*, 75–80. [CrossRef]
37. Agarwal, A.K.; Das, L.M. Biodiesel Development and Characterization for Use as a Fuel in Compression Ignition Engines. *J. Eng. Gas Turbines Power.* **2001**, *123*, 440–447. [CrossRef]
38. Rosha, P.; Mohapatra, S.K.; Mahla, S.K.; Cho, H.; Chauhan, B.S.; Dhir, A. Effect of compression ratio on combustion, performance, and emission characteristics of compression ignition engine fueled with palm (B20) biodiesel blend. *Energy* **2019**, *178*, 676–684. [CrossRef]
39. Asokan, M.A.; Senthur Prabu, S.; Bade, P.K.K.; Nekkanti, V.M.; Gutta, S.S.G. Performance, combustion and emission characteristics of juliflora biodiesel fuelled DI diesel engine. *Energy* **2019**, *173*, 883–892. [CrossRef]
40. Musthafa, M.M.; Kumar, T.A.; Mohanraj, T.; Chandramouli, R. A comparative study on performance, combustion and emission characteristics of diesel engine fuelled by biodiesel blends with and without an additive. *Fuel* **2018**, *225*, 343–348. [CrossRef]
41. Can, Ö. Combustion characteristics, performance and exhaust emissions of a diesel engine fueled with a waste cooking oil biodiesel mixture. *Energy Convers. Manag.* **2014**, *87*, 676–686. [CrossRef]
42. Dueso, C.; Muñoz, M.; Moreno, F.; Arroyo, J.; Gil-Lalaguna, N.; Bautista, A.; Gonzalo, A.; Sánchez, J.L. Performance and emissions of a diesel engine using sunflower biodiesel with a renewable antioxidant additive from bio-oil. *Fuel* **2018**, *234*, 276–285. [CrossRef]
43. Canakci, M. Combustion characteristics of a turbocharged DI compression ignition engine fueled with petroleum diesel fuels and biodiesel. *Bioresour. Technol.* **2007**, *98*, 1167–1175. [CrossRef]

44. Murillo, S.; Míguez, J.L.; Porteiro, J.; Granada, E.; Morán, J.C. Performance and exhaust emissions in the use of biodiesel in outboard diesel engines. *Fuel* **2007**, *86*, 1765–1771. [CrossRef]
45. Özener, O.; Yüksek, L.; Ergenç, A.T.; Özkan, M. Effects of soybean biodiesel on a DI diesel engine performance, emission and combustion characteristics. *Fuel* **2014**, *115*, 875–883. [CrossRef]
46. Emiroğlu, A.O.; Şen, M. Combustion, performance and emission characteristics of various alcohol blends in a single cylinder diesel engine. *Fuel* **2018**, *212*, 34–40. [CrossRef]
47. Abed, K.A.; Gad, M.S.; El Morsi, A.K.; Sayed, M.M.; Elyazeed, S.A. Effect of biodiesel fuels on diesel engine emissions. *Egypt. J. Pet.* **2019**, *28*, 183–188. [CrossRef]
48. Ong, H.C.; Masjuki, H.H.; Mahlia, T.M.I.; Silitonga, A.S.; Chong, W.T.; Yusaf, T. Engine performance and emissions using Jatropha curcas, Ceiba pentandra and Calophyllum inophyllum biodiesel in a CI diesel engine. *Energy.* **2014**, *69*, 427–445. [CrossRef]